remote sensing

MDPI

Article

Global Accuracy Comparison from Multi-Source NO_2 Products Based on Pandora Observations

Shuaimin Wang [1,2,†], Yu Guo [1,†], Jiajia Zhang [2,3], Anzhou Zhao [1,*], Yujing Xu [1] and Dongli Wang [1]

[1] School of Mining and Geomatics Engineering, Hebei University of Engineering, Handan 056038, China; wsm1949@sina.com (S.W.); insidekoss@163.com (Y.G.); xuyujing@hebeu.edu.cn (Y.X.); wangdongli@hebeu.edu.cn (D.W.)
[2] Key Laboratory of Intelligent Meteorological Observation Technology, China Meteorological Administration, Beijing 100081, China; sunyi_12_12@sina.com
[3] Meteorological Technology and Equipment Center of Hebei Province, Hebei Meteorological Bureau, Shijiazhuang 050022, China
* Correspondence: zhaoanzhou@hebeu.edu.cn
† These authors contributed equally to this work.

Highlights

What are the main findings?

- TROPOMI exhibits the highest accuracy among the four global $TOTNO_2$ products (R = 0.88, RMSE = 4.83 Pmolec·cm^{-2}), while CAMS reanalysis shows the largest bias and error (MB = −4.91 Pmolec·cm^{-2}, RMSE = 9.15 Pmolec·cm^{-2}).
- All four $TOTNO_2$ products (OMI, TROPOMI, GOME-2, CAMS) systematically underestimate Pandora ground-based observations and follow a clear "winter-high, summer-low" seasonal cycle.

What are the implications of the main findings?

- Linear bias correction reduces systematic errors by more than 79% and lowers RMSE by 4–28%, significantly improving the consistency between satellite/CAMS data and ground-based measurements.
- The superior accuracy and stability of TROPOMI make it a suitable reference for calibrating coarser-resolution products like CAMS, facilitating multi-source NO_2 data fusion and air quality applications.

Abstract

Effective evaluation of the accuracy of multi-source NO_2 products from different satellites and reanalysis is of great significance for data fusion and application. Based on NO_2 observation data from Pandora stations worldwide, we verify and compare the accuracy of the total column density of NO_2 ($TOTNO_2$) from OMI, TROPOMI, GOME-2 satellites and CAMS reanalysis. The mean biases of the four $TOTNO_2$ datasets relative to the Pandora station observation data are all negative, indicating that all four $TOTNO_2$ products show systematic underestimation with respect to Pandora. Overall, TROPOMI has the highest correlation (R = 0.88) and the smallest root mean square error (RMSE = 4.83 Pmolec·cm^{-2}), suggesting that among the four $TOTNO_2$ products, the accuracy of TROPOMI $TOTNO_2$ is higher compared with the other $TOTNO_2$ products. The accuracies of OMI and GOME-2 are in the middle, while the performance of CAMS is the poorest. The $TOTNO_2$ values and accuracies from the four $TOTNO_2$ products both show a seasonal characteristic. Among the four $TOTNO_2$ products, the accuracy is higher in summer, and the error increases in autumn and winter. After performing linear fitting correction on the four NO_2 products, the mean biases of each data are reduced by more than 79%, and the RMSE decreases by

Check for updates

Academic Editor: Carmine Serio

Received: 30 April 2026
Revised: 20 June 2026
Accepted: 22 June 2026
Published: 24 June 2026

Copyright: © 2026 by the authors. Licensee MDPI, Basel, Switzerland. This article is an open access article distributed under the terms and conditions of the Creative Commons Attribution (CC BY) license.

4–28%. The consistency of the four TOTNO_2 products with the ground-based observation data is significantly improved.

Keywords: NO_2; Pandora; OMI; TROPOMI; GOME-2

1. Introduction

NO_2 is not only an important trace gas pollutant in the atmosphere [1], participating in the control process of ozone (O_3) and hydroxyl radicals in the troposphere, but also a key primary air pollutant and a key precursor for ozone formation [2,3]. The sources of NO_2 can be traced back to natural processes and human activities. Natural sources of NO_2 mainly include soil emissions, lightning, wildfires and volcanic activities. Human emission sources are highly concentrated in fossil fuel consumption in the fields of traffic and industrial processes [4,5]. When NO_2 concentration is too high, it not only has a serious impact on air quality [6] but also poses a threat to the human respiratory system [7]. Therefore, accurately monitoring and analyzing the spatio-temporal distribution and the concentration changes of NO_2 in the atmosphere is of vital importance for pollution control and policy-making for human health [5].

There are various NO_2 data sources, such as ground-based station data, satellite observation data, and reanalysis data [3,8], but there are differences among them. Ground-based station data can provide high-precision and high-time-resolution column gas concentration data and are widely used for satellite data verification [9]. However, due to the uneven distribution and limited number of observation stations, large-scale detection cannot be achieved and the cost is relatively high. Satellite NO_2 monitoring, with its advantages of global coverage, continuous observation and providing long-term series data, has become an important technology for monitoring global atmospheric NO_2 concentration. At present, many atmospheric composition monitoring satellites have been successfully launched internationally. For example, the European Remote-Sensing Satellite-2 (ERS-2) was launched by the European Space Agency (ESA) in 1995. ERS-2 is equipped with the Global Ozone Monitoring Experiment (GOME), and this Satellite ceased operation in 2003 [10]. The Environmental Satellite (ENVISAT), launched in 2002, is equipped with a Scanning Imaging Absorption SpectroMeter for Atmospheric CHartographY (SCIAMACHY), which aims to provide data on the concentration of trace gases in the troposphere and stratosphere [11]. The Aura satellite launched by National Aeronautics and Space Administration (NASA) is equipped with an Ozone Monitoring Instrument (OMI) sensor [12]. Subsequently, the Global Ozone Monitoring Experiment-2 (GOME-2) was carried by the Meteorological Operational Satellite-A/B (MetOp-A/B) Satellite [13]. The Tropospheric Monitoring Instrument (TROPOMI), carried by the Sentinel-5 Precursor (Sentinel-5P) satellite, was launched in 2017 with the mission of atmospheric monitoring, marking a significant improvement in the spatial resolution of satellite monitoring of NO_2 [14]. At present, OMI, GOME-2 and TROPOMI are in normal operation. Furthermore, the reanalysis dataset of the Copernicus Atmosphere Monitoring Service (CAMS) generates a continuous spatiotemporal data field with high spatial resolution and high temporal resolution [15]. Ground-based NO_2 observation data have high accuracy and thus are often used as the benchmark for satellite accuracy verification.

At present, satellite observations can provide long-term and wide-range NO_2 data, which are widely used for the analysis of spatiotemporal variations in NO_2 [16–19], but their accuracy and reliability are unknown. Therefore, it is necessary to verify the accuracy of the multiple NO_2 data. Judd et al. took the NO_2 data of the Pandora station as the reference

value to comparatively analyze the accuracy of the Sentinel-5 Precursor (S-5P) NO_2 data in the New York area. The results showed that there is a significant correlation between the Pandora and TROPOMI NO_2 data [20]. Herman et al. analyzed the accuracy of OMI NO_2 data based on Pandora station NO_2 data, and the results show that OMI systematically underestimates the amount of NO_2 in the atmosphere [21]. Celarier et al. comprehensively verified the OMI NO_2 product based on Systeme d'Analyse par Observations Zenithales (SAOZ) and DOAS ground observation data. The results indicate that OMI NO_2 has a good correlation with ground measurements, but there is a systematic underestimation bias [22]. Peters et al. conducted a comparative analysis of the NO_2 data of GOME-2 and SCIAMACHY based on MAX-DOAS data and found that there is only about 1% difference between SCIAMACHY and GOME-2, indicating a good consistency between the two NO_2 data [23]. Wang et al. verified the accuracy of GOME-2A/B using MAX-DOAS tropospheric NO_2 data from Wuxi, China, from 2011 to 2014, and found that the estimated values of GOME-2A/B products are systematically higher, approximately 30% higher [24]. Pinardi et al. verified the NO_2 accuracy of the GOME-2 satellite based on MAX-DOAS ground-based data. The results show that the correlation between GOME-2 NO_2 data and ground observation NO_2 data in clean areas is above 0.8, and the consistency is good [25]. Gruzdev et al. compared the NO_2 data from Russian ground stations with the NO_2 column concentration of the OMI satellite. The results show that the correlation coefficient between the NO_2 column concentration of OMI and that of the ground observation is 0.92, indicating a good consistency between the two types of data [26]. Douros et al. compared the NO_2 concentrations in Europe using CAMS and TROPOMI and found that there is a high consistency between the tropospheric NO_2 column concentrations of the two datasets in summer, with the relative differences in most cities not exceeding 15%. In winter, there are significant differences in column concentrations in most parts of Europe, with the maximum relative difference reaching up to 50% [8].

At present, on the one hand, the accuracy verification of NO_2 products from remote sensing or reanalysis mainly focuses on the evaluation and comparison of one or two NO_2 products. The differences in temporal matching principles of the remote sensing NO_2 data and ground reference NO_2 data with different time coverage ranges in different papers make it impossible to directly verify and compare different NO_2 products. On the other hand, the accuracy verification and comparative analysis of NO_2 data from different satellites are of great significance for the application of NO_2 data and data fusion. At present, there are relatively few studies on the accuracy verification and analysis of different satellite data under the same conditions, including the same station and the same temporal matching principle, and there are also few studies on the accuracy verification and comparison of CAMS reanalysis data and different satellites under the same conditions. In addition, there are certain differences in the accuracy and applicability of different satellites and reanalysis NO_2 products in different regions and at different times around the world. Therefore, in this paper, the total column density of NO_2 ($TOTNO_2$) products of OMI, TROPOMI, GOME-2 and CAMS are verified and compared from August 2021 to July 2023 using global Pandora station data as reference values based on the same temporal matching principle, and bias correction models for four $TOTNO_2$ products have been established.

2. Data and Methods

2.1. Data

2.1.1. Pandora Data

The Pandonia Global Network (PGN) is a collaborative project between NASA (Washington, DC, USA) and ESA (Paris, France), which uses ground-based Pandora spectrometers to monitor trace gases, such as nitrogen dioxide, ozone, sulfur dioxide and

formaldehyde [27]. The main purpose of PGN is to provide long-term mass observations of the total column density and vertical resolution concentration of a series of trace gases [28]. The Pandora instrument is a solar spectrophotometer. Its observation conditions are that the Solar Zenith Angle (SZA) is less than 80°. The wavelength range is 280–525 nm, and it can obtain high signal-to-noise ratio spectral data in the ultraviolet band and the visible light-ultraviolet mixed band separately. The minimum integration time is 4 ms, the direct solar field of view angle is 1.6° [29], and the inversion is performed approximately every 2 min [30]. The data used in this study were sourced from https://data.hetzner.pandonia-global-network.org/ (accessed on 21 June 2026) and filtered based on the following criteria: Normalized Root Mean Square > 0.05, quality flags selected as Q0, Q1, Q10, and Q11, SolarZenithAngle < 75, and NO_2 value > 0.

2.1.2. OMI NO_2 Product

OMI is a hyperspectral imaging spectrometer operating in a sun-synchronous orbit [31], providing global observational data of ozone and major atmospheric pollutant gases such as NO_2 and SO_2, with a spatial resolution of 13 × 24 km [32], a transit time of close to 13:45 local time [33], and a time range from 1 October 2004 to 1 January 2025. In this paper we use OMI NO_2 vertical column data from August 2021 to July 2023, the data can be downloaded at NASA's Goddard space flight center (Greenbelt, MD, USA) for free access (https://disc.gsfc.nasa.gov/datasets/OMI_MINDS_NO2_1.1/summary?keywords=NO2 (accessed on 21 June 2026)), by filtering and retaining data with cloud cover less than 0.5, solar zenith angle less than 70°, positive NO_2 column amounts, and quality flags (VcdQualityFlags and XTrackQualityFlags) set to zero.

2.1.3. TROPOMI NO_2 Product

TROPOMI is an instrument carried on the Sentinel-5 Precursor satellite launched by the European Space Agency (ESA) with a sun-synchronous orbit, which was successfully launched on 13 October 2017 [34,35]. TROPOMI is mainly used to obtain the vertical column data of key components in the atmosphere, including NO_2, ozone (O_3), sulfur dioxide (SO_2), formaldehyde (HCHO), methane (CH_4), and carbon monoxide (CO), etc. TROPOMI has a scanning width of 2600 km, enabling daily global coverage, and its transit time is approximately 13:00 local time [33]. Its spatial resolution is relatively high, at 3.5 km × 7 km, and has been improved to 3.5 km × 5.5 km since 6 August 2019 [36]. TROPOMI can provide both near-real-time data and offline data. TROPOMI NO_2 data can be downloaded from the ESA's official website (https://dataspace.copernicus.eu/ (accessed on 21 June 2026)), filtering and retaining data with cloud cover less than 0.5, solar zenith angle less than 70°, a qa_value of at least 0.75, and a positive nitrogendioxide_total_column.

2.1.4. GOME-2 NO_2 Product

The Metop series satellites (METOP-A, METOP-B and METOP-C), as an important component of the Global meteorological observation network, are equipped with a variety of high-precision instruments, including the GOME-2, Infrared Atmospheric Sounding Interferometer (IASI) and Advanced Microwave Sounding Unit-A (AMSU-A) [37]. On 17 September 2012, the Metop-B satellite was successfully launched, with an orbital altitude of 817 km [38,39]. The Metop-B satellite was developed by the European Organisation for the Exploitation of Meteorological Satellites (EUMETSAT, Darmstadt, Germany). The meteorological satellite system managed by EUMETSAT is designed to provide high-quality atmospheric monitoring and meteorological data, supporting global climate change research and meteorological forecasting efforts.

The GOME-2 carried by the Metop-B satellite plays a significant role in the monitoring of nitrogen dioxide and is one of the main instruments for atmospheric composition

monitoring. It can measure multiple atmospheric pollutants such as O_3, NO_2, and sulfate aerosols, and provide high-precision data covering the world [35]. This paper screens the vertical column NO_2 concentration data that meet the criteria of cloud cover < 50% and solar zenith angle < 70°, and NO_2 concentration > 0.

2.1.5. CAMS NO_2 Product

Copernicus Atmosphere Monitoring Service Reanalysis (CAMSRA) is a global atmospheric composition reanalysis dataset produced by the European Centre for Medium-Range Weather Forecasts (ECMWF, Reading, UK) [39], also known as ECMWF's Fourth-generation Atmospheric Composition Reanalysis (EAC4). This data reanalysis process is not subject to the time limit of real-time forecasting, thus enabling the collection of more observational data and the application of an improved inversion algorithm to historical observations, which enhances the quality of the final product [38]. The advantage of this dataset lies in that even in regions with sparse observations, the model can provide reasonable estimated values and offer long-term, globally covered data records in a unified format, which greatly facilitates the spatio-temporal analysis and trend research of atmospheric components. This study uses the global NO_2 total column density data provided by CAMS, with a temporal resolution of 3 h and a spatial resolution of 0.75° × 0.75° [36], which can be obtained from the official website (https://ads.atmosphere.copernicus.eu/ (accessed on 21 June 2026)).

The information of OMI, TROPOMI, GOME-2 satellite data, Pandora ground-based station and CAMS reanalysis data is shown in Table 1.

Table 1. Information on a multi-source satellite, CAMS and Pandora ground station.

Type	Instrument	Data Version	Spatial Resolution/km	Time Resolution	Time Range
Ground-based	Pandora	-	-	2 min	2010–present
Satellite observation	OMI	MINDS v1.1	13 × 24	98.8 min	1 October 2004–1 January 2025
	TROPOMI	HiR v2	3.5 × 5.5	1 d	13 October 2017–present
	GOME-2	TM4-NO2A v 2.3	80 × 40	1 d	17 September 2012–10 January 2024
CAMS reanalysis	-	EAC4 v2	80 × 80	3 h	1 December 2003–31 December 2024

2.2. Research Methods

This study aims to evaluate and compare the accuracies of the $TOTNO_2$ products from OMI, TROPOMI, GOME-2 satellite data and CAMS reanalysis data based on the Pandora station, explore their spatio-temporal distribution characteristics, and perform linear correction. We only use the Pandora $TOTNO_2$ data to independently verify the accuracy of the $TOTNO_2$ products from OMI, TROPOMI, GOME-2 and CAMS, and do not compare the $TOTNO_2$ among OMI, TROPOMI, GOME-2 and CAMS. When one kind of satellite $TOTNO_2$ data is verified based on Pandora, it is completely independent of the other two kinds of satellite $TOTNO_2$ data. This study is mainly divided into three steps. Firstly, qualified data are selected, and the satellite data or CAMS data are matched with the ground station data according to certain temporal and spatial matching principles. Secondly, the temporal and spatial distribution characteristics of $TOTNO_2$ are analyzed, and the accuracy of the matching results is evaluated and analyzed. Finally, through linear correction of the data, the systematic errors of the data are processed to obtain more accurate results. The research process is shown in Figure 1.

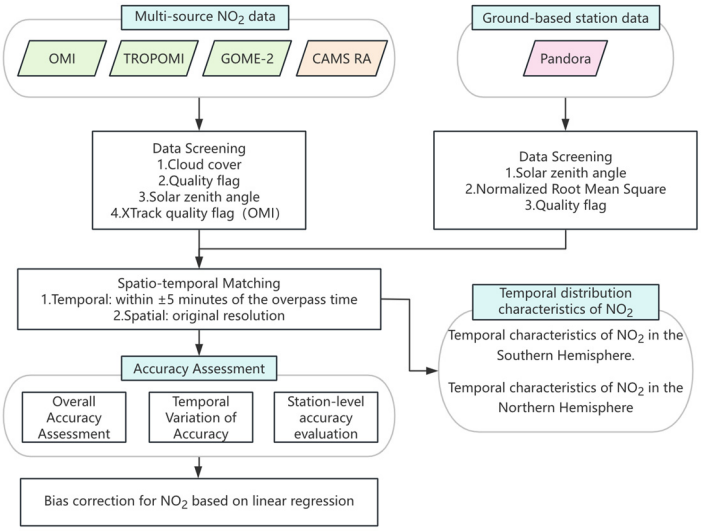


Figure 1. Flow chart of $TOTNO_2$ accuracy evaluation.

2.2.1. Data Matching Method

In terms of time, the mean value of the $TOTNO_2$ from Pandora station observation data within 5 min before or after the satellite transit time or the CAMS data time is selected. Spatially, with the ground station as the center, the satellite and CAMS data within the distance range of native resolution around the station are selected to obtain the mean value. Finally, better matching data pairs of the stations and satellite or CAMS data are obtained. Based on the matching results, a comprehensive comparative analysis of different data sources is conducted.

2.2.2. Screening Method

Based on the data from 148 Pandora stations worldwide, we conduct a systematic accuracy verification of four $TOTNO_2$ products from TROPOMI, OMI, GOME-2 and CAMS. The low- and medium-quality Pandora observation data contain large uncertain errors that compromise data accuracy evaluation. Stations with too few valid data pairs cannot provide statistically meaningful results, while a high requirement on the number of matching data pairs would leave too few usable Pandora stations. Therefore, we selected only Pandora stations with high-quality observations and more than 10 satellite-matched data pairs for accuracy assessment, and eventually, 46 Pandora stations with better matching effects were obtained for in-depth analysis, thus ensuring the reliability and representativeness of the verification results. The global distribution of the 46 stations is shown in Figure 2.

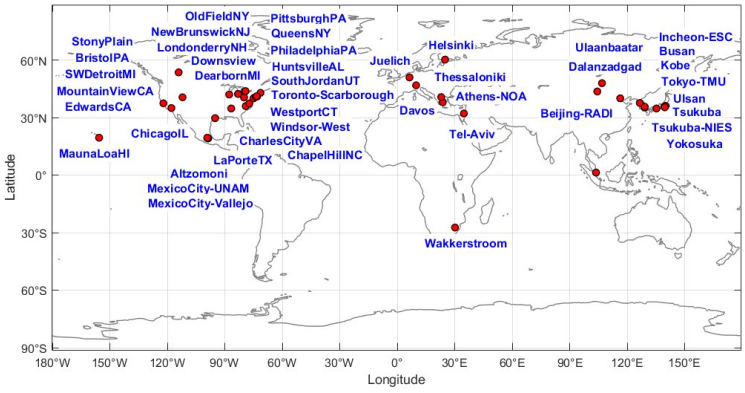


Figure 2. Distribution map of Pandora stations worldwide after screening.

2.2.3. Statistical Indicators

To quantitatively evaluate the consistency and differences among different data sources, the following statistical indicators are adopted in this study: Mean Bias (MB), Root Mean Square Error (RMSE), Standard Deviation (STD), and Correlation Coefficient (R).

$$MB = \frac{1}{n}\sum_{i=1}^{n}(TOTNO2_{sate,i} - TOTNO2_{site,i}) \quad (1)$$

$$RMSE = \sqrt{\frac{1}{n}\sum_{i=1}^{n}(TOTNO2_{sate,i} - TOTNO2_{site,i})^2} \quad (2)$$

$$STD = \sqrt{\frac{1}{n}\sum_{i-1}^{n}(TOTNO2_{sate,i} - TOTNO2_{site,i} - \overline{TOTNO2_{sate} - TOTNO2_{site}})^2} \quad (3)$$

$$R = \frac{\sum_{i=1}^{n}(TOTNO2_{sate,i} - \overline{TOTNO2_{sate}})(TOTNO2_{site,i} - \overline{TOTNO2_{site}})}{\sqrt{\sum_{i=1}^{n}(TOTNO2_{sate,i} - \overline{TOTNO2_{site}})^2 \sum_{i=1}^{n}(TOTNO2_{sate,i} - \overline{TOTNO2_{site}})^2}} \quad (4)$$

where $TOTNO2_{sate}$ represents the total column density of nitrogen dioxide for satellites/CAMS reanalysis, and $TOTNO2_{site}$ represents the total column density of nitrogen dioxide for the Pandora station.

2.2.4. Bias Correction Method

Firstly, in the matching $TOTNO_2$ dataset, a random sampling strategy is employed to divide the training set and the validation set. A total of 80% of the samples are used for linear fitting model construction, while 20% are reserved for independent validation to ensure the generalization ability of the corrected model and the objectivity of the evaluation. Subsequently, on the training set, the linear regression is conducted using the observation values from the Pandora station as the dependent variable and the satellite observations or reanalysis data as the independent variable, which is shown in Equation (5).

$$TOTNO2_{site} = a \times TOTNO2_{sate} + b \quad (5)$$

3. Results

3.1. Comparison of the Temporal Characteristics of NO_2 Products Three Kinds of Satellite and CAMS Reanalysis with Those of the Pandora Station

In order to more accurately analyze the time variation patterns of the four $TOTNO_2$ products and the $TOTNO_2$ from ground-based observation stations, the differences in time variation patterns between the Northern and Southern Hemispheres are taken into account. The temporal characteristics of $TOTNO_2$ products from OMI, TROPOMI, GOME-2 and CAMS, as well as Pandora from August 2021 to July 2023 in the Southern Hemisphere and the Northern Hemisphere are shown in Figure 3.

The temporal characteristics of $TOTNO_2$ products from OMI, TROPOMI, GOME-2 and CAMS, as well as Pandora from August 2021 to July 2023, are shown in Figure 3. As shown in Figure 3, overall, the four $TOTNO_2$ products exhibit a consistent trend of change with the data from the Pandora station, all showing distinctly seasonal characteristics. The $TOTNO_2$ concentration is relatively low in summer, gradually increases in autumn and winter, and reaches its peak in winter. In the Northern Hemisphere, ground-based $TOTNO_2$ is higher than the three satellite products and CAMS in most cases. There are too

few ground-based observation stations in the Southern Hemisphere, so this phenomenon is not obvious.

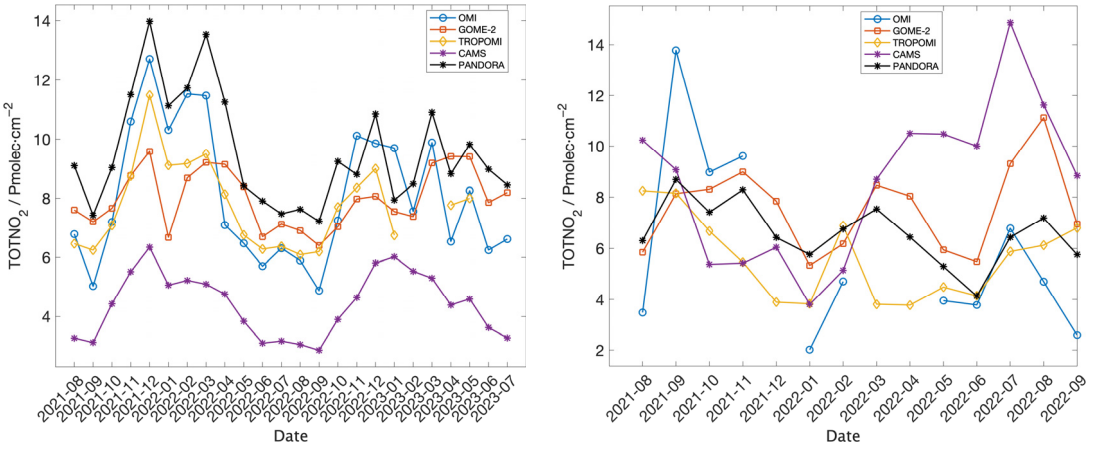


Figure 3. Comparison of the temporal characteristics of NO_2 products from OMI, TROPOMI, GOME-2 and CAMS, as well as Pandora station. (**a**) Northern Hemisphere; (**b**) Southern Hemisphere.

Among the $TOTNO_2$ datasets from the three satellites, the $TOTNO_2$ of TROPOMI and OMI are the closest, and they also have the same temporal characteristics as Pandora. However, the consistency between GOME-2 and Pandora's NO_2 products lies between those of other satellite data and CAMS.

3.2. Accuracy Assessment of Multi-Source NO_2 Products Based on Pandora Ground-Based Observations

3.2.1. Overall Accuracy Assessment of NO_2 Products

The scatter plots and box plots comparing the four $TOTNO_2$ data products (OMI, TROPOMI, GOME-2 and CAMS) with the ground-based observations at the global Pandora stations are shown in Figures 4 and 5, respectively.

Figure 4 shows that the correlation between TROPOMI and Pandora $TOTNO_2$ observations is the highest (R = 0.88), and the RMSE value of 4.83 Pmolec·cm^{-2} is the smallest among the four products, indicating the best consistency between TROPOMI and ground-based observations. The mean bias between TROPOMI and Pandora is −1.48 Pmolec·cm^{-2}, which indicates that there is a systematic deviation in TROPOMI $TOTNO_2$, which is significantly underestimated compared to the Pandora station. The RMSE and STD of OMI are similar to those of TROPOMI, indicating that the accuracies of the two $TOTNO_2$ products are comparable. The mean absolute bias of OMI is slightly larger than that of TROPOMI, indicating that the systematic bias of the OMI $TOTNO_2$ product is smaller compared to that of TROPOMI.

Figure 5 shows that all four $TOTNO_2$ products exhibit a systematic negative bias. The median biases of the four $TOTNO_2$ products are all less than 0. The results indicate that the overall values of these four $TOTNO_2$ products are underestimated compared to the ground-based $TOTNO_2$ products. The upper quartile of the CAMS bias is less than 0, indicating that the CAMS $TOTNO_2$ product is significantly underestimated by more than 75% compared to ground-based observations. The median bias between OMI and GOME-2 is similar, but the dispersion of OMI is smaller, indicating that the OMI NO_2 product has better accuracy and stability. The maximum and minimum biases of TROPOMI are both relatively small, and the bias range of TROPOMI is more concentrated, indicating that the accuracy and stability of the TROPOMI NO_2 product are better compared to the other three products.

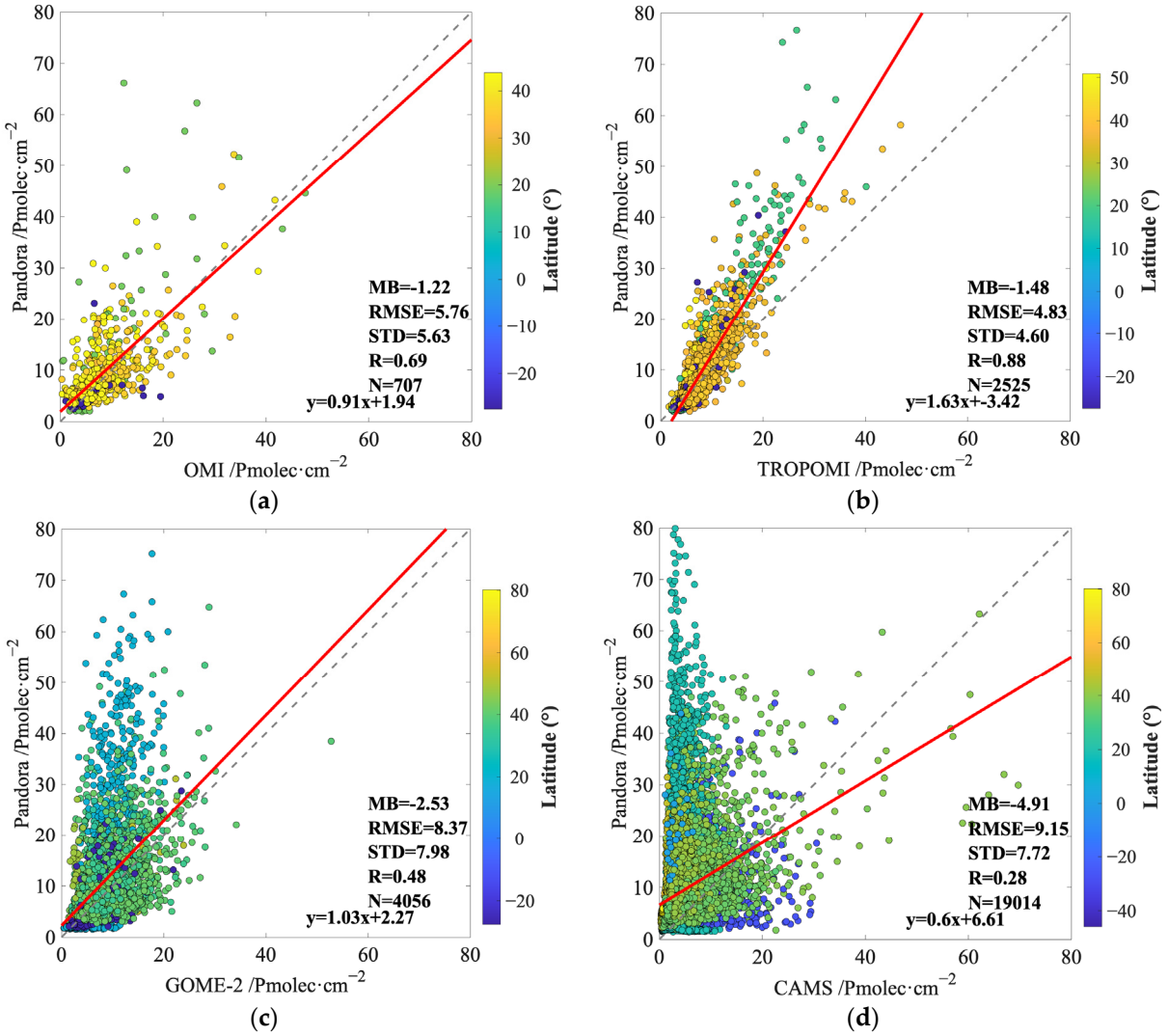


Figure 4. Scatter plots of NO_2 data relative to Pandora ground-based observations. (**a**) OMI versus Pandora; (**b**) TROPOMI versus Pandora; (**c**) GOME-2 versus Pandora; (**d**) CAMS reanalysis versus Pandora.

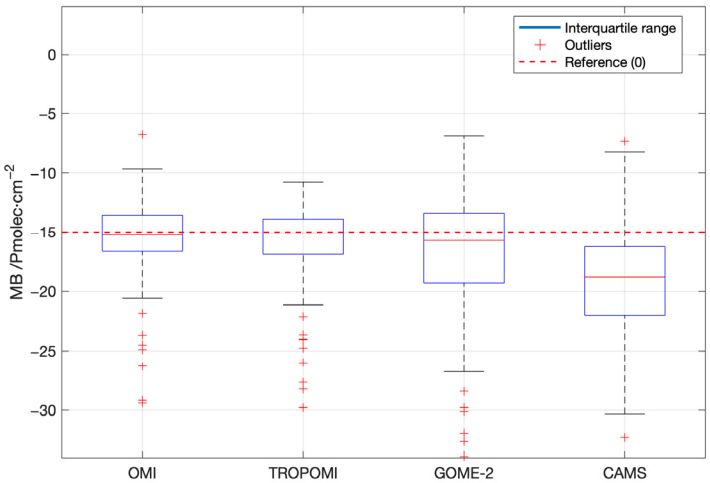


Figure 5. Box plots of bias distributions of four types of NO_2 data.

3.2.2. The Accuracy of the Four NO_2 Products Changes over Time

The monthly root mean square error results of the four NO_2 products (OMI, TROPOMI, GOME-2 and CAMS) relative to the observations at the Pandora station are shown in Figure 6. Due to the scarcity of stations in the Southern Hemisphere, this analysis is conducted based on the stations in the Northern Hemisphere.

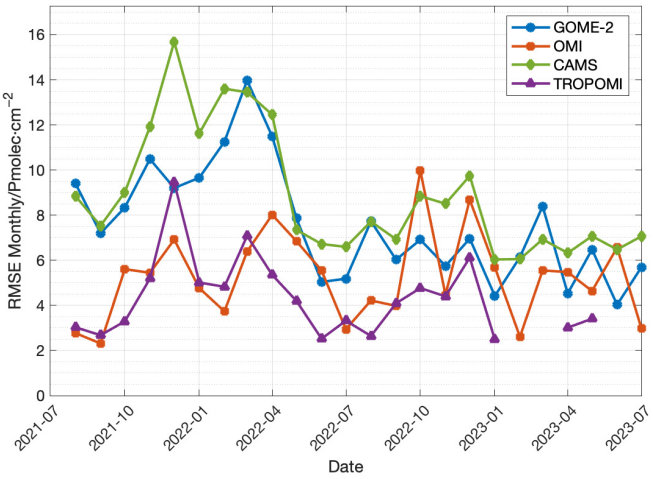


Figure 6. Monthly mean RMSE change in the four $TOTNO_2$ products relative to ground-based observations.

Figure 6 shows that the monthly RMSE values of the four $TOTNO_2$ products show seasonal fluctuations. The RMSE values of the four $TOTNO_2$ are generally higher in winter. In December 2021, the RMSE of GOME-2, OMI, CAMS and TROPOMI reached 9.20 Pmolec·cm^{-2}, 6.92 Pmolec·cm^{-2}, 15.69 Pmolec·cm^{-2} and 9.46 Pmolec·cm^{-2}, respectively, while they significantly decreased in summer. In July 2022, the RMSEs of GOME-2, OMI, CAMS and TROPOMI drop to 5.18 Pmolec·cm^{-2}, 2.94 Pmolec·cm^{-2}, 6.59 Pmolec·cm^{-2} and 3.32 Pmolec·cm^{-2}, respectively.

Table 2 indicates that the number of collocation pairs shows an uneven distribution over the period from August 2021 to July 2023. Due to the fact that the number of collocation pairs of the four datasets in the period from August 2022 to July 2023 is generally smaller than that of the four datasets in the period from August 2021 to July 2022, the seasonal variation in RMSE from August 2022 to July 2023 is not as obvious as that from August 2021 to July 2022.

Table 2. The number of collocation pairs of OMI, TROPOMI, GOME-2 and CAMS relative to Pandora.

Month	GOME-2	OMI	CAMS	TROPOMI
2021-08	219	23	1190	155
2021-09	258	16	1141	179
2021-10	246	19	909	138
2021-11	304	25	817	169
2021-12	204	16	553	153
2022-01	111	26	580	133
2022-02	207	28	709	112
2022-03	195	29	812	115
2022-04	203	19	833	96

Table 2. *Cont.*

Month	GOME-2	OMI	CAMS	TROPOMI
2022-05	164	37	1040	93
2022-06	139	43	1077	80
2022-07	168	29	1110	90
2022-08	174	25	1087	133
2022-09	207	23	1002	165
2022-10	231	36	895	180
2022-11	192	20	710	157
2022-12	106	50	517	121
2023-01	80	9	293	48
2023-02	40	13	338	0
2023-03	94	24	373	0
2023-04	81	32	443	67
2023-05	129	63	662	68
2023-06	90	29	597	0
2023-07	89	42	657	0

3.2.3. Station-Level Accuracy Evaluation from NO_2 Products

Figures 7–10 present the station-level accuracy evaluation statistics of four $TOTNO_2$ products from OMI, TROPOMI, GOME-2 and CAMS relative to 46 Pandora stations worldwide. At most observation stations, Figure 8 indicates that the RMSE of the CAMS $TOTNO_2$ product is significantly higher than that of the other three satellite products. Moreover, the correlation coefficient of the CAMS $TOTNO_2$ product at most observation stations is significantly lower than that of the other three satellite products. The results show that the accuracy of CAMS $TOTNO_2$ is lower than that of other satellite products. TROPOMI $TOTNO_2$ consistently demonstrates the highest and most stable accuracy at most stations. The accuracy of OMI $TOTNO_2$ is generally stable, with relatively high accuracy at many stations (such as Beijing-RADI), similar to that of TROPOMI. However, as shown in Figure 11, the error of OMI significantly increases in some highly polluted cities (such as Incheon-ESC, Yokosuka). The station-level accuracy of GOME-2 varies greatly, and the errors are the highest at some stations, especially at high-pollution stations such as Incheon-ESC.

From the perspective of spatial distribution patterns, at most of the stations, four NO_2 products exhibit good consistency, and the root mean square error values of these four NO_2 products at most stations are either relatively large or relatively small. The findings indicate that the RMSE values of the four products are highly correlated with the quality and concentration of the station observations. The errors of the four $TOTNO_2$ products are relatively small at low NO_2 stations (such as Dalanzadgad), and the consistency with respect to Pandora stations is good. However, in regions with high NO_2 concentrations, especially in urban clusters in East Asia and North America, the errors of the four $TOTNO_2$ products increase. The differences between CAMS and satellite data are particularly prominent among them.

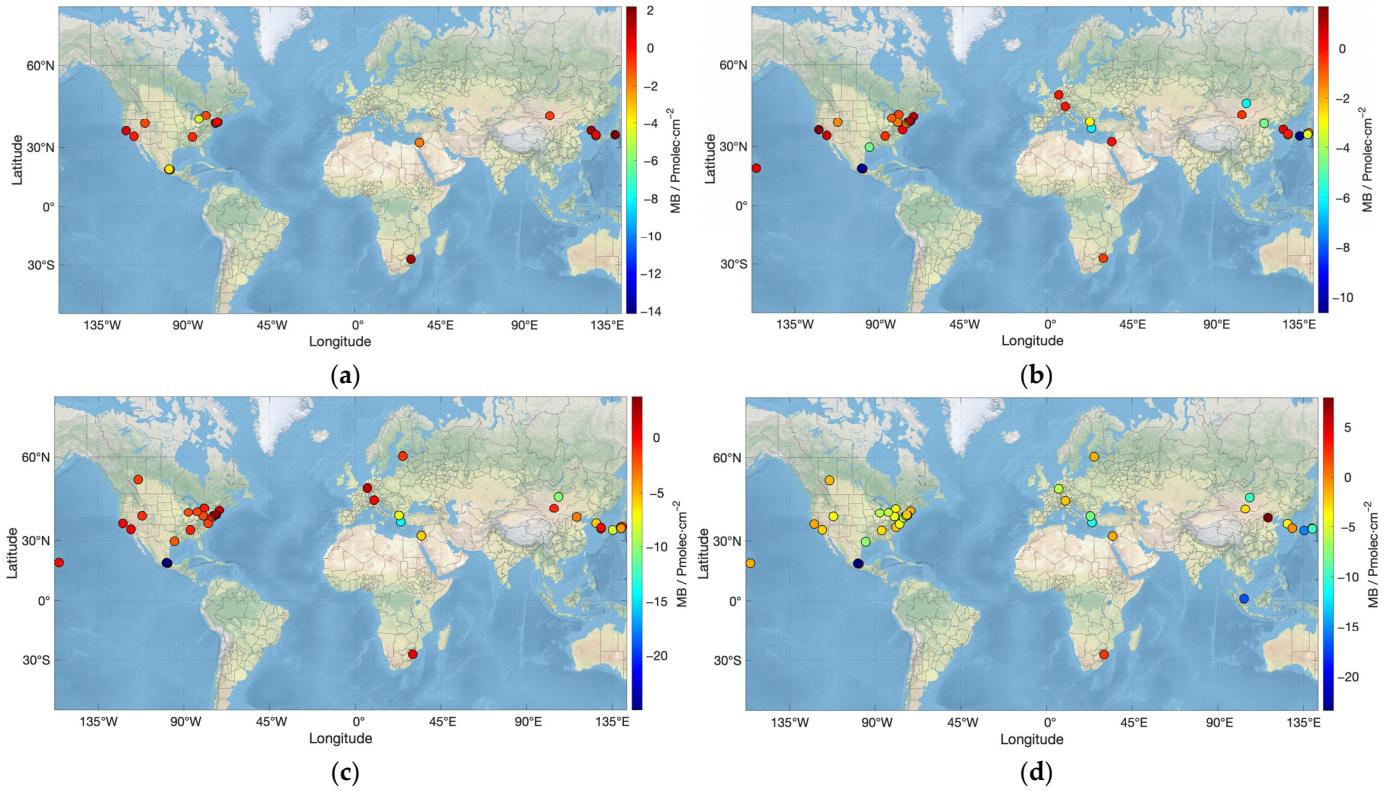


Figure 7. MB distribution of $TOTNO_2$ data from (**a**) OMI, (**b**) TROPOMI, (**c**) GOME-2 and (**d**) CAMS relative to Pandora ground-based observations.

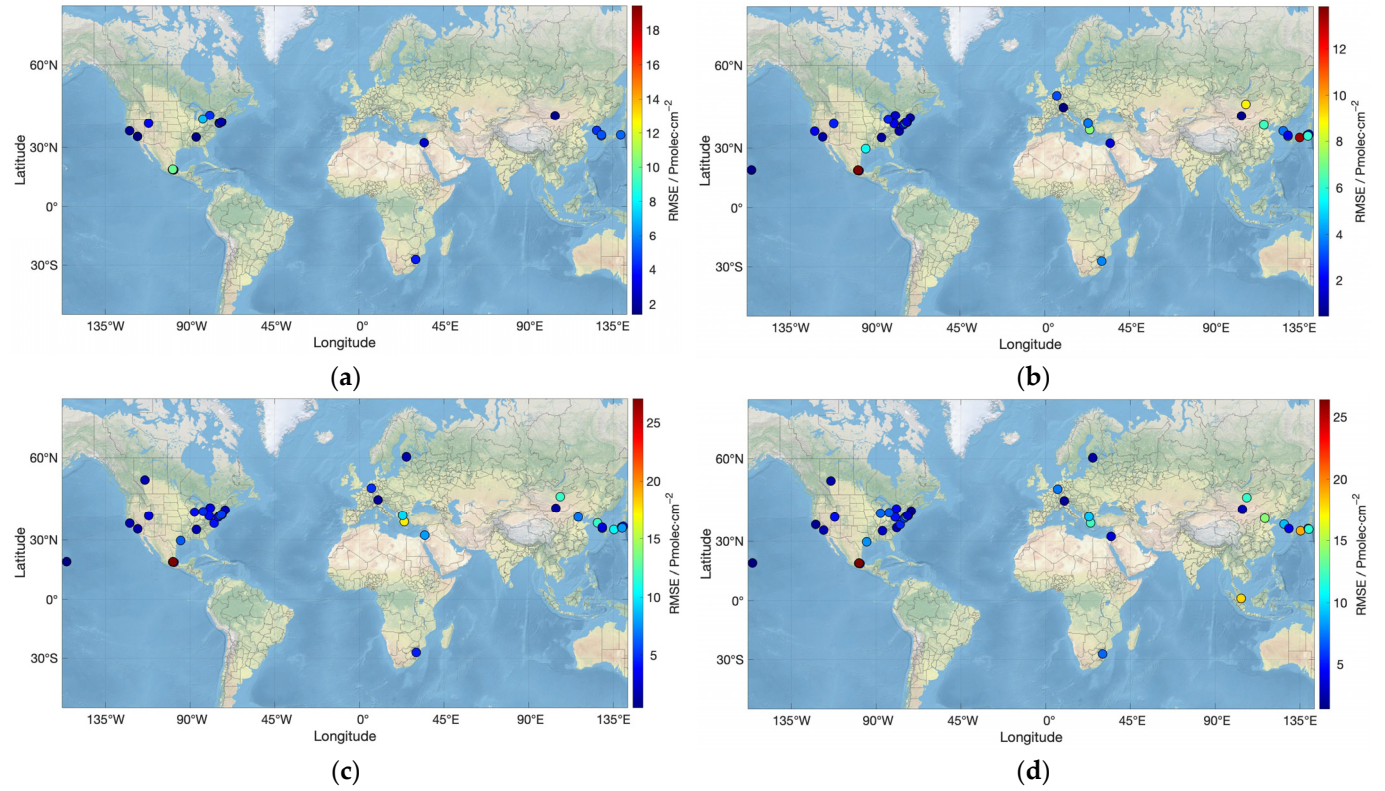


Figure 8. RMSE distribution of $TOTNO_2$ data from (**a**) OMI, (**b**) TROPOMI, (**c**) GOME-2 and (**d**) CAMS relative to Pandora ground-based observations.

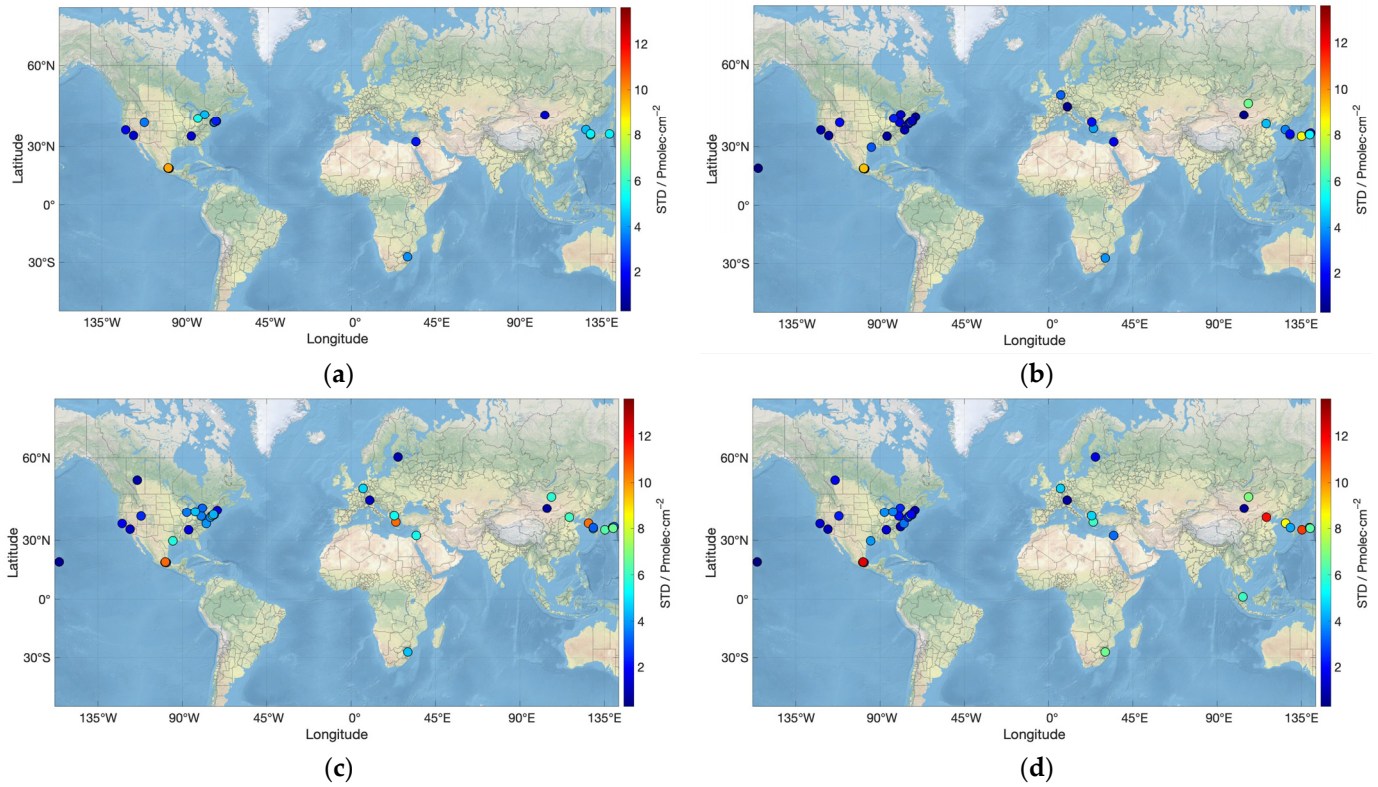


Figure 9. STD distribution of $TOTNO_2$ data from (**a**) OMI, (**b**) TROPOMI, (**c**) GOME-2 and (**d**) CAMS relative to Pandora ground-based observations.

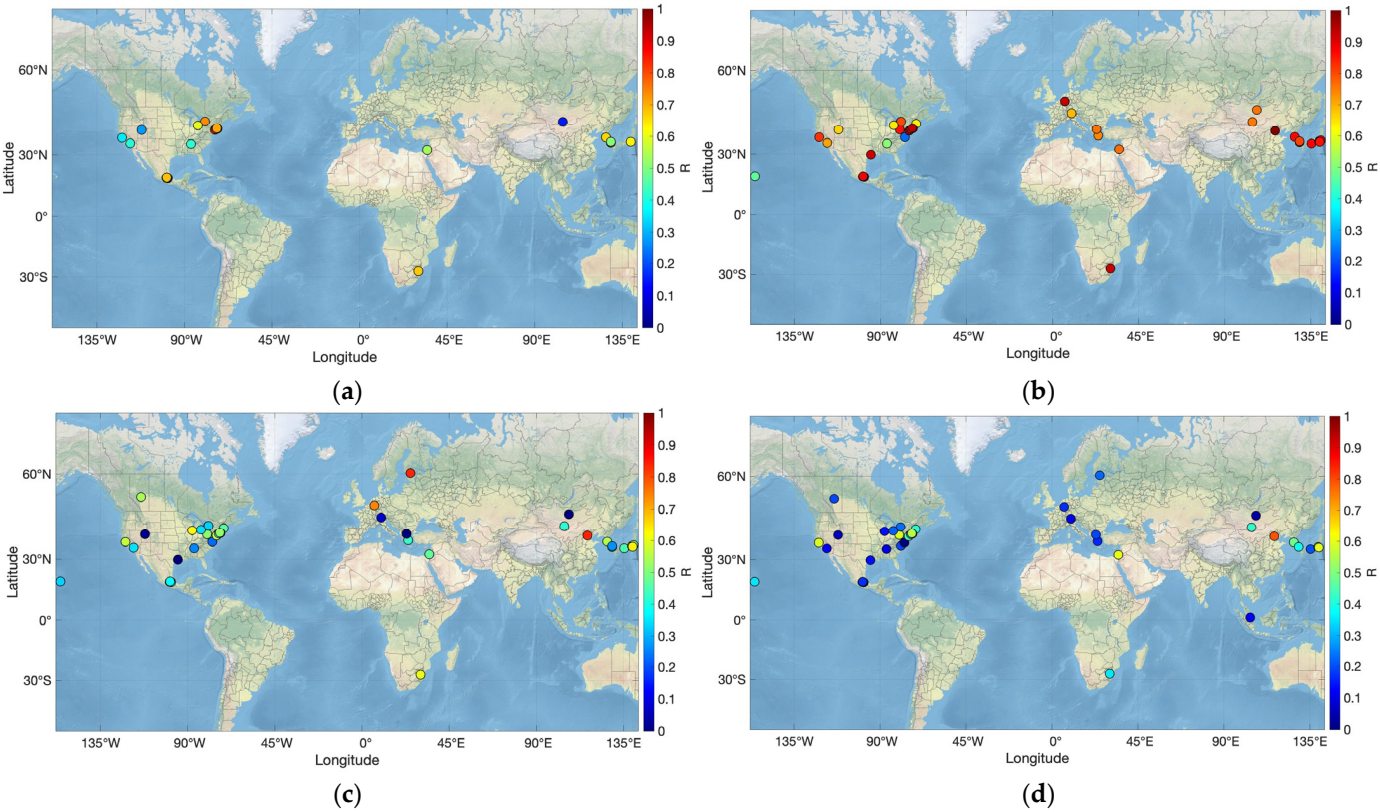


Figure 10. R distribution of $TOTNO_2$ data from (**a**) OMI, (**b**) TROPOMI, (**c**) GOME-2 and (**d**) CAMS relative to Pandora ground-based observations.

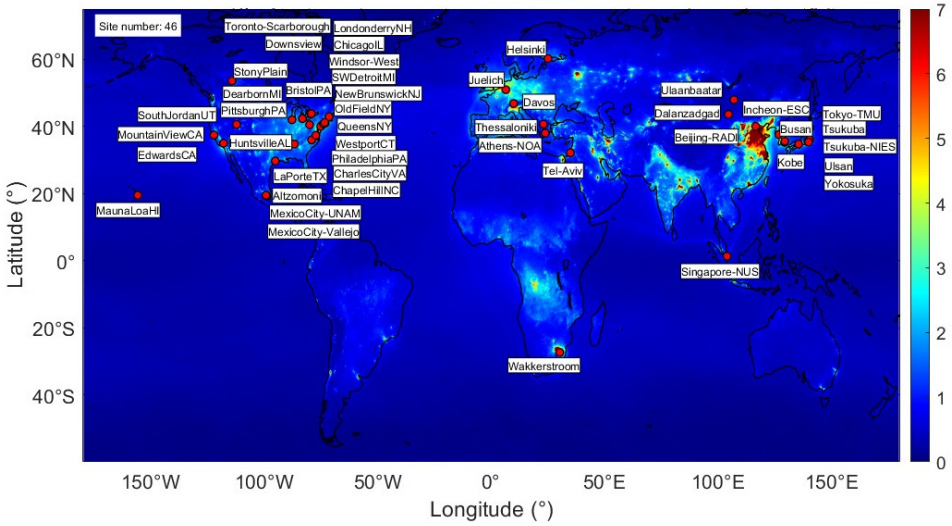


Figure 11. The 2022 global mean map of NO_2 in the troposphere.

3.3. Analysis of Bias Correction for TOTNO$_2$ Products from OMI, TROPOMI, GOME-2 and CAMS

The biases of four $TOTNO_2$ products from OMI, TROPOMI, GOME-2 and CAMS are corrected based on a linear fitting model. A total of 80% of matching results from four $TOTNO_2$ products are randomly selected for linear fitting to obtain the linear fitting equation. Then, the remaining 20% of the four $TOTNO_2$ products is used for verification. The accuracy comparison of the four $TOTNO_2$ products before and after bias correction is shown in Table 3. Table 3 shows that the MB values of the four NO_2 products are all less than 0.25 Pmolec.cm^{-2}, indicating that after correction, the mean biases of OMI, TROPOMI, GOME-2 and CAMS have significantly decreased by more than 79%. After correction, the RMSE values of OMI, TROPOMI, GOME-2 and CAMS decreased by 4%, 28%, 5% and 17%, respectively. The standard deviation (STD) and correlation coefficient (R) of the corrected data changed relatively little.

Table 3. Comparison of accuracy before and after correction of NO_2 products.

Type	Bias Correction	MD /Pmolec·cm^{-2}	RMSE /Pmolec·cm^{-2}	STD /Pmolec·cm^{-2}	R
OMI	Before correction	−1.06	5.05	4.77	0.74
	After correction	0.22	4.87	4.70	0.74
TROPOMI	Before correction	−1.57	4.70	4.43	0.91
	After correction	−0.16	3.38	3.38	0.91
GOME-2	Before correction	−2.40	7.87	7.50	0.51
	After correction	0.16	7.50	7.50	0.51
CAMS	Before correction	−4.77	8.88	7.49	0.31
	After correction	0.14	7.36	7.35	0.31

4. Discussion

4.1. Discussion on the Change in Accuracy Before and After the Downgrade of OMI

Due to the severe degradation of detector response and polarization sensitivity of OMI since 2019, the OMI $TOTNO_2$ product has been corrected for the period after 2019. To compare the accuracy of the corrected OMI $TOTNO_2$ products (post-2019) with that of the products before 2019, we use observation data from the same Pandora stations over

the same length of time (two years) to evaluate the data from 2017 to 2018 and August 2021–July 2023, respectively, as shown in Figure 12.

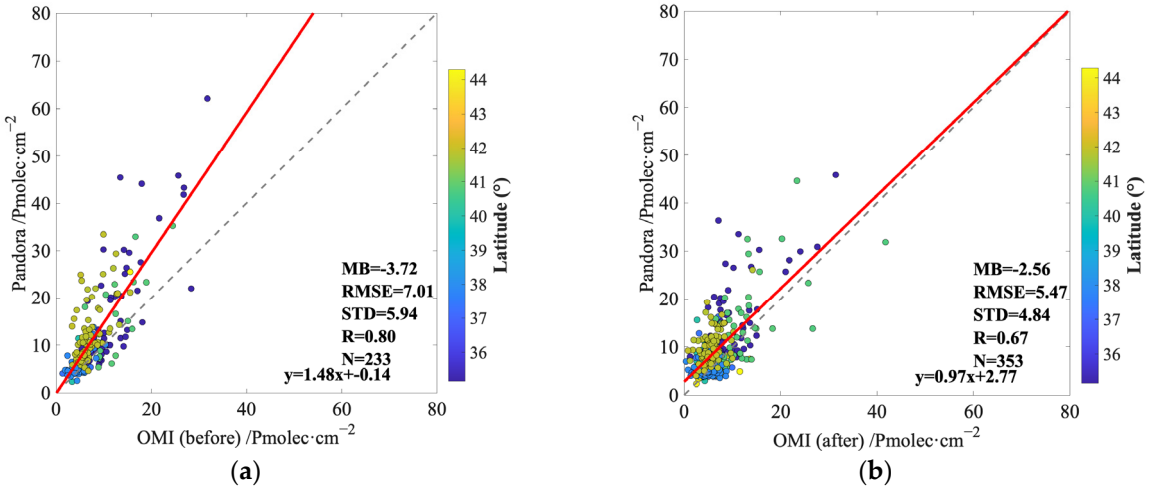


Figure 12. Change in accuracy (**a**) before and (**b**) after the downgrade of OMI.

Figure 12 indicates that the MB, RMSE, and STD of the OMI TOTNO$_2$ products from 2017 to 2018 are smaller than those of the OMI products from August 2021 to July 2023. The findings indicate that the accuracy of the OMI TOTNO$_2$ products from 2017 to 2018 is slightly superior to that of the OMI products from August 2021 to July 2023. The main reasons are as follows: Firstly, the OMI TOTNO$_2$ data products after 2019 have undergone bias correction [40]. Secondly, we select high-quality OMI NO$_2$ products and exclude abnormal row data, so the accuracy of the OMI TOTNO$_2$ product does not change much.

4.2. Discussion on Temporal Characteristics and Systematic Underestimation

The seasonal variation in NO$_2$ is mainly influenced by both meteorological conditions and human emissions. In summer, the intense solar radiation accelerates the photolysis reaction of NO$_2$, while the higher atmospheric boundary layer facilitates the vertical dispersion of pollutants. In contrast, during winter, the increase in coal burning for heating leads to higher NO$_2$ emissions, combined with a lower atmospheric boundary layer and frequent inversion phenomena, making it difficult for pollutants to disperse, thereby resulting in a cumulative increase in NO$_2$ concentration.

The differences among satellite products mainly result from various factors such as inversion algorithms, instrument resolution, and observation quality. The main reasons for the general underestimation of actual TOTNO$_2$ concentration by satellite NO$_2$ products may be as follows. On the one hand, NO$_2$ is mainly concentrated near the ground surface, and the reduced sensitivity of satellites to signals near the ground surface leads to an underestimation of the NO$_2$ concentration near the ground surface. On the other hand, high-pollution data are systematically excluded during the cloud screening process. Similarly, the underestimated satellite TOTNO$_2$ product is assimilated into the CAMS reanalysis product, resulting in a relatively low accuracy of the CAMS TOTNO$_2$ product.

The better accuracy and stability of the TROPOMI TOTNO$_2$ product compared to the other three products may be attributed to the superior spatial resolution that enables it to capture the spatial heterogeneity of urban NO$_2$ more precisely. The differences between satellites may stem from factors such as their spatial resolution and inversion algorithms.

4.3. Discussion on Seasonal Accuracy Variation

The seasonal variation in RMSE—higher in winter and lower in summer—arises from multiple physical mechanisms that affect satellite retrievals and reanalysis data assimilation.

In winter, several factors jointly increase retrieval uncertainties. First, aerosol interference is more pronounced: higher aerosol optical thickness (AOT) due to anthropogenic emissions (e.g., heating, stagnant conditions) enhances photon scattering and absorption, altering the effective optical path and biasing NO_2 slant column density estimates. Second, air mass factor (AMF) uncertainties grow under low solar elevation angles (winter overpass times) and high aerosol loading, as the AMF depends on the assumed vertical profile of NO_2 and aerosols—deviations from the a priori profile introduce systematic errors. Third, boundary layer dynamics in winter often produce strong temperature inversions, trapping pollutants near the surface and creating sharp vertical gradients that are poorly captured by the coarse vertical resolution of model priors. Fourth, cloud screening effects are more challenging: while clouds can reduce data availability, partial cloud cover and sub-pixel clouds are more frequent in winter mid-latitudes, leading to misclassification and residual cloud contamination that degrades retrieval accuracy. Finally, differences in satellite overpass times relative to solar zenith angle (SZA) matter—higher SZA in winter increases the optical path length, reducing sensitivity to near-surface NO_2 and amplifying the impact of all the above uncertainties. In contrast, summer offers cleaner atmospheric conditions (lower AOT), smaller SZA, more stable boundary layers, and fewer cloud interference issues, all of which improve the accuracy of $TOTNO_2$ products. Thus, the observed RMSE seasonality is a direct consequence of these physically intertwined factors, rather than a simple correlation with pollutant concentration alone.

4.4. Discussion on Bias Correction

The results show that the linear fitting model has a significant effect on correcting the systematic errors of $TOTNO_2$ products. After correction, the RMSE of the four $TOTNO_2$ products has significantly decreased, suggesting a significant improvement in the overall accuracy. Among the four products, the $TOTNO_2$ product of the corrected CAMS has the most significant improvement in accuracy. The standard deviation (STD) and correlation coefficient (R) of the corrected data changed relatively little, indicating that the correction process mainly eliminates the systematic errors while still being influenced by random errors. This is because random errors are affected by various uncertain factors, including the meteorological conditions, surface reflectivity, and aerosol interference, which do not have a stable systematic change pattern, and are difficult to predict and eliminate through simple linear models. However, bias correction still improved the accuracy of satellite $TOTNO_2$ products, making them more consistent with ground-based observations.

However, the limitations of the linear correction approach should be acknowledged. Satellite NO_2 retrieval errors are often nonlinear and strongly modulated by season, aerosol loading, surface reflectivity, boundary layer conditions, and pollution levels. The linear regression model employed here is overly simplistic and does not account for these complex factors. Consequently, the physical meaning and generalizability of the linear correction remain limited. Future work should explore more sophisticated, physically based or machine-learning methods to better capture the nonlinear nature of retrieval errors across varying environmental conditions.

5. Conclusions

NO_2 participates in the photochemical cycle and serves as an important precursor for ozone (O_3) and secondary aerosols (such as nitrate particles), directly influencing regional air quality and atmospheric oxidation capacity. Based on the $TOTNO_2$ observation data from the global Pandora stations as the reference value, the temporal variation characteristics of $TOTNO_2$ products from OMI, TROPOMI, GOME-2 and CAMS reanalysis data and their consistency with Pandora are investigated. We systematically compare and analyze

the consistency of four $TOTNO_2$ products with Pandora and use the linear fitting method to correct the bias of the four kinds of $TOTNO_2$ products. The main conclusions are as follows:

(1) The four $TOTNO_2$ data sources relative to the Pandora observations generally show systematic underestimation, with negative mean bias values. Among them, TROPOMI $TOTNO_2$ products perform best, with the highest correlation coefficient (average R = 0.88) and the smallest RMSE value (RMSE = 4.83 Pmolec·cm^{-2}), reflecting its advantage in capturing the distribution of urban NO_2 with high spatial resolution. The accuracies of the OMI and GOME-2 $TOTNO_2$ products are comparable and intermediate. The $TOTNO_2$ data from CAMS reanalysis shows the largest bias and RMSE (MB = −4.91 Pmolec·cm^{-2}, RMSE = 9.15 Pmolec·cm^{-2}), and the results are unstable in different regions, indicating a significant discrepancy between the model simulation and the ground-based observation values.

(2) In terms of the temporal variation characteristics, an obvious seasonality, characterized by higher $TOTNO_2$ values in winter and lower $TOTNO_2$ values in summer, is evident in all four $TOTNO_2$ products, and this variation agrees well with the Pandora observation. The increase in $TOTNO_2$ concentration in winter is primarily attributed to increased anthropogenic emissions (particularly from heating combustion), reduced photochemical loss rates, and a marked decrease in atmospheric dispersion capacity caused by adverse meteorological conditions such as temperature inversions. In summer, due to enhanced photolysis and the elevation of the boundary layer, the concentration drops to the lowest level. From the perspective of seasonal variation in $TOTNO_2$ product accuracy, each data source has the smallest bias and the highest correlation in summer, while the RMSE and STD generally increase in autumn and winter, which may be related to the decrease in the solar elevation angle in winter and the aggravation of aerosol influence.

(3) In terms of bias correction, the correction method based on linear fitting effectively reduces the systematic bias of the four types of $TOTNO_2$ data. After correction, the mean bias values of OMI, TROPOMI, GOME-2 and CAMS decreased by 79%, 90%, 93% and 97%, respectively, and the root mean square error values decreased by 4%, 28%, 5% and 17%, respectively. The results indicate that the systematic bias values of the four kinds of $TOTNO_2$ products have been significantly reduced and the accuracies have significantly improved. However, the random error (STD) and correlation of the four kinds of $TOTNO_2$ products do not change significantly. The four kinds of $TOTNO_2$ products after correction are overall closer to the ground-based observations, providing a reliable foundation for the fusion and application of multi-source NO_2 data.

Author Contributions: Conceptualization, S.W. and A.Z.; methodology, S.W., Y.X. and J.Z.; software, Y.G.; validation, Y.G. and Y.X.; formal analysis, Y.G.; investigation, S.W. and Y.G.; resources, S.W., J.Z. and D.W.; data curation, Y.G.; writing—original draft preparation, Y.G. and S.W.; writing—review and editing, S.W.; visualization, Y.G.; supervision, A.Z., J.Z. and D.W.; project administration, S.W. and Y.X.; funding acquisition, S.W. and A.Z. All authors have read and agreed to the published version of the manuscript.

Funding: Natural Science Foundation of Hebei Province of China (grant numbers No. D2023402024), National Natural Science Foundation of China (grant numbers No. 42171212), Open Research Project of the Key Open Laboratory for Intelligent Meteorological Observation Technology of the China Meteorological Administration (grant numbers No. ZNGC2024MS18), Science Research Project of Hebei Education Department (grant numbers No. JCZX2026037).

Data Availability Statement: The OMI data can be accessed at the following URL: https://disc.gsfc.nasa.gov/datasets/OMI_MINDS_NO2_1.1/summary?keywords=NO2 (accessed on 21 June

2026). The TROPOMI data can be accessed at the following URL: https://dataspace.copernicus.eu/ (accessed on 21 June 2026). The CAMS data can be accessed at the following URL: https://ads.atmosphere.copernicus.eu/ (accessed on 21 June 2026). The Pandora data can be accessed at the following URL: https://data.hetzner.pandonia-global-network.org/ (accessed on 21 June 2026).

Acknowledgments: The authors would like to thank the Pandonia Global Network (PGN) for providing the Pandora data, and the ECMWF and NASA for providing the CAMS and satellite data. No generative AI was used in the preparation of this manuscript.

Conflicts of Interest: The authors declare no conflicts of interest.

Abbreviations

The following abbreviations are used in this manuscript:

NO_2	nitrogen dioxide
ERS-2	European Remote-Sensing Satellite-2
ESA	European Space Agency
GOME	Global Ozone Monitoring Experiment
ENVISAT	Environmental Satellite
SCIAMACHY	Scanning Imaging Absorption SpectroMeter for Atmospheric CHartographY
NASA	National Aeronautics and Space Administration
OMI	Ozone Monitoring Instrument
GOME-2	Global Ozone Monitoring Experiment-2
MetOp-A/B	Meteorological Operational Satellite-A/B
TROPOMI	Tropospheric Monitoring Instrument
S-5P	Sentinel-5 Precursor
CAMS	Copernicus Atmosphere Monitoring Service
SAOZ	Systeme d'Analyse par Observations Zenithales
$TOTNO_2$	total column density of NO_2
PGN	Pandonia Global Network
SZA	Solar Zenith Angle
O_3	ozone
SO_2	sulfur dioxide
HCHO	formaldehyde
CH_4	methane
CO	carbon monoxide
IASI	Infrared Atmospheric Sounding Interferometer
EUMETSAT	Exploitation of Meteorological Satellites
CAMSRA	Copernicus Atmosphere Monitoring Service Reanalysis
ECMWF	European Centre for Medium-Range Weather Forecasts
EAC4	ECMWF's Fourth-generation Atmospheric Composition Reanalysis
MB	Mean Bias
RMSE	Root Mean Square Error
STD	Standard Deviation
R	Correlation Coefficient

References

1. Boersma, K.F.; Eskes, H.J.; Brinksma, E.J. Error analysis for tropospheric NO_2 retrieval from space. *J. Geophys. Res. Atmos.* **2004**, *109*, D04311. [CrossRef]
2. Cheng, S.; Ma, J.; Cheng, W.; Yan, P.; Zhou, H.; Zhou, L.; Yang, P. Tropospheric NO_2 vertical column densities retrieved from ground-based MAX-DOAS measurements at Shangdianzi regional atmospheric background station in China. *J. Environ. Sci.* **2019**, *80*, 186–196.
3. Zhang, Y.; Wei, Y.; de Leeuw, G.; Liu, O.; Chen, Y.; Lv, Y.; Zhang, Y.; Li, Z. Relation between total vertical column density and near-surface NO_2 based on in situ and Pandora ground-based remote sensing observations. *Atmos. Chem. Phys.* **2025**, *25*, 10643–10660.

4. Hesterberg, T.W.; Bunn, W.B.; McClellan, R.O.; Hamade, A.K.; Long, C.M.; Valberg, P.A. Critical review of the human data on short-term nitrogen dioxide (NO_2) exposures: Evidence for NO_2 no-effect levels. *Crit. Rev. Toxicol.* **2009**, *39*, 743–781. [PubMed]
5. Van Der A, R.; Eskes, H.; Boersma, K.; Van Noije, T.; Van Roozendael, M.; De Smedt, I.; Peters, D.; Meijer, E. Trends, seasonal variability and dominant NOx source derived from a ten year record of NO_2 measured from space. *J. Geophys. Res. Atmos.* **2008**, *113*, D04302. [CrossRef]
6. Alberts, W.M. Indoor air pollution: NO, NO_2, CO, and CO_2. *J. Allergy Clin. Immunol.* **1994**, *94*, 289–295. [CrossRef] [PubMed]
7. Lamsal, L.N.; Krotkov, N.A.; Celarier, E.A.; Swartz, W.H.; Pickering, K.E.; Bucsela, E.J.; Gleason, J.F.; Martin, R.V.; Philip, S.; Irie, H.; et al. Evaluation of OMI operational standard NO_2 column retrievals using in situ and surface-based NO_2 observations. *Atmos. Chem. Phys.* **2014**, *14*, 11587–11609. [CrossRef]
8. Douros, J.; Eskes, H.; van Geffen, J.; Boersma, K.F.; Compernolle, S.; Pinardi, G.; Blechschmidt, A.-M.; Peuch, V.-H.; Colette, A.; Veefkind, P. Comparing Sentinel-5P TROPOMI NO_2 column observations with the CAMS regional air quality ensemble. *Geosci. Model Dev.* **2022**, *2022*, 509–534. [CrossRef]
9. Di Bernardino, A.; Mevi, G.; Iannarelli, A.M.; Falasca, S.; Cede, A.; Tiefengraber, M.; Casadio, S. Temporal variation of NO_2 and O_3 in Rome (Italy) from Pandora and in situ measurements. *Atmosphere* **2023**, *14*, 594. [CrossRef]
10. Burrows, J.P.; Weber, M.; Buchwitz, M.; Rozanov, V.; Ladstätter-Weißenmayer, A.; Richter, A.; DeBeek, R.; Hoogen, R.; Bramstedt, K.; Eichmann, K.-U.; et al. The global ozone monitoring experiment (GOME): Mission concept and first scientific results. *J. Atmos. Sci.* **1999**, *56*, 151–175. [CrossRef]
11. Bracher, A.; Bovensmann, H.; Bramstedt, K.; Burrows, J.; Von Clarmann, T.; Eichmann, K.-U.; Fischer, H.; Funke, B.; Gil-López, S.; Glatthor, N.; et al. Cross comparisons of O_3 and NO_2 measured by the atmospheric ENVISAT instruments GOMOS, MIPAS, and SCIAMACHY. *Adv. Space Res.* **2005**, *36*, 855–867. [CrossRef]
12. Garane, K.; Koukouli, M.-E.; Verhoelst, T.; Lerot, C.; Heue, K.-P.; Fioletov, V.; Balis, D.; Bais, A.; Bazureau, A.; Dehn, A.; et al. TROPOMI/S5P total ozone column data: Global ground-based validation and consistency with other satellite missions. *Atmos. Meas. Tech.* **2019**, *12*, 5263–5287.
13. Argyrouli, A.; Lutz, R.; Romahn, F.; Molina García, V.; Loyola, D.; Seo, S.; Valks, P.; De Smedt, I.; Boersma, F.; Tilstra, L.G.; et al. Comparison of Cloud Parameters from GOME-2 and Assessment of Cloud Impact on Tropospheric NO_2 and HCHO Retrievals. *Environ. Sci. Proc.* **2023**, *26*, 203. [CrossRef]
14. Cersosimo, A.; Serio, C.; Masiello, G. TROPOMI NO_2 tropospheric column data: Regridding to 1 km grid-resolution and assessment of their consistency with in situ surface observations. *Remote Sens.* **2020**, *12*, 2212. [CrossRef]
15. Inness, A.; Flemming, J.; Heue, K.-P.; Lerot, C.; Loyola, D.; Ribas, R.; Valks, P.; Van Roozendael, M.; Xu, J.; Zimmer, W. Monitoring and assimilation tests with TROPOMI data in the CAMS system: Near-real-time total column ozone. *Atmos. Chem. Phys.* **2019**, *19*, 3939–3962.
16. Zhang, Y.; Shi, M.; Chen, J.; Fu, S.; Wang, H. Spatiotemporal variations of NO_2 and its driving factors in the coastal ports of China. *Sci. Total Environ.* **2023**, *871*, 162041. [CrossRef] [PubMed]
17. Ma, C.; Ju, T.; Wang, Q.; Li, F.; Zhang, Y.; Zhang, G. Spatiotemporal variations of tropospheric NO_2 in Lanzhou for the period 2009–2018 based on satellite remote sensing. *Atmos. Pollut. Res.* **2021**, *12*, 206–216. [CrossRef]
18. Wang, C.; Wang, T.; Wang, P. The spatial–temporal variation of tropospheric NO_2 over China during 2005 to 2018. *Atmosphere* **2019**, *10*, 444. [CrossRef]
19. Zhao, Z.; Lu, Y.; Zhan, Y.; Cheng, Y.; Yang, F.; Brook, J.R.; He, K. Long-term spatiotemporal variations in surface NO_2 for Beijing reconstructed from surface data and satellite retrievals. *Sci. Total Environ.* **2023**, *904*, 166693. [CrossRef] [PubMed]
20. Judd, L.M.; Al-Saadi, J.A.; Szykman, J.J.; Valin, L.C.; Janz, S.J.; Kowalewski, M.G.; Eskes, H.J.; Veefkind, J.P.; Cede, A.; Mueller, M.; et al. Evaluating Sentinel-5P TROPOMI tropospheric NO_2 column densities with airborne and Pandora spectrometers near New York City and Long Island Sound. *Atmos. Meas. Tech.* **2020**, *13*, 6113–6140. [CrossRef] [PubMed]
21. Herman, J.; Abuhassan, N.; Kim, J.; Kim, J.; Dubey, M.; Raponi, M.; Tzortziou, M. Underestimation of column NO_2 amounts from the OMI satellite compared to diurnally varying ground-based retrievals from multiple PANDORA spectrometer instruments. *Atmos. Meas. Tech.* **2019**, *12*, 5593–5612. [CrossRef]
22. Celarier, E.A.; Brinksma, E.J.; Gleason, J.F.; Veefkind, J.P.; Cede, A.; Herman, J.R.; Ionov, D.; Goutail, F.; Pommereau, J.-P.; Lambert, J.-C.; et al. Validation of Ozone Monitoring Instrument nitrogen dioxide columns. *J. Geophys. Res. Atmos.* **2008**, *113*, D15S15. [CrossRef]
23. Peters, E.; Wittrock, F.; Großmann, K.; Frieß, U.; Richter, A.; Burrows, J. Formaldehyde and nitrogen dioxide over the remote western Pacific Ocean: SCIAMACHY and GOME-2 validation using ship-based MAX-DOAS observations. *Atmos. Chem. Phys.* **2012**, *12*, 11179–11197.
24. Wang, Y.; Beirle, S.; Lampel, J.; Koukouli, M.; De Smedt, I.; Theys, N.; Li, A.; Wu, D.; Xie, P.; Liu, C.; et al. Validation of OMI, GOME-2A and GOME-2B tropospheric NO_2, SO_2 and HCHO products using MAX-DOAS observations from 2011 to 2014 in Wuxi, China: Investigation of the effects of priori profiles and aerosols on the satellite products. *Atmos. Chem. Phys.* **2017**, *17*, 5007–5033.

25. Pinardi, G.; Lambert, J.; Granville, J.; Roozendael, M.; Delcloo, A.; Backer, H.; Valks, P.; Hao, N. Overview of the validation of GOME-2 total and tropospheric NO_2 columns. In Proceedings of the EUMETSAT Meteorological Satellite Conference, Córdoba, Spain, 20–24 September 2010.
26. Gruzdev, A.N.; Elokhov, A.S. Validation of Ozone Monitoring Instrument NO_2 measurements using ground based NO_2 measurements at Zvenigorod, Russia. *Int. J. Remote Sens.* **2010**, *31*, 497–511. [CrossRef]
27. Ghahremanloo, M.; Nowlan, C.; Abad, G.G.; Garraffo, C.; Liu, X.; Wang, H.; Henderson, B.; Baumann, E.; Valin, L.; Geddes, J.A.; et al. Comprehensive Analysis of Bias in TEMPO NO_2 Column Densities Through Pandora Observations. *J. Geophys. Res. Atmos.* **2025**, *130*, e2025JD044150. [CrossRef] [PubMed]
28. Liu, O.; Li, Z.; Lin, Y.; Fan, C.; Zhang, Y.; Li, K.; Zhang, P.; Wei, Y.; Chen, T.; Dong, J.; et al. Evaluation of the first year of Pandora NO_2 measurements over Beijing and application to satellite validation. *Atmos. Meas. Tech.* **2024**, *17*, 377–395. [CrossRef]
29. Herman, J.; Cede, A.; Spinei, E.; Mount, G.; Tzortziou, M.; Abuhassan, N. NO_2 column amounts from ground-based Pandora and MFDOAS spectrometers using the direct-sun DOAS technique: Intercomparisons and application to OMI validation. *J. Geophys. Res. Atmos.* **2009**, *114*, D13307.
30. Reed, A.J.; Thompson, A.M.; Kollonige, D.E.; Martins, D.K.; Tzortziou, M.A.; Herman, J.R.; Berkoff, T.A.; Abuhassan, N.K.; Cede, A. Effects of local meteorology and aerosols on ozone and nitrogen dioxide retrievals from OMI and pandora spectrometers in Maryland, USA during DISCOVER-AQ 2011. *J. Atmos. Chem.* **2015**, *72*, 455–482. [PubMed]
31. Duncan, B.N.; Yoshida, Y.; de Foy, B.; Lamsal, L.N.; Streets, D.G.; Lu, Z.; Pickering, K.E.; Krotkov, N.A. The observed response of Ozone Monitoring Instrument (OMI) NO_2 columns to NOx emission controls on power plants in the United States: 2005–2011. *Atmos. Environ.* **2013**, *81*, 102–111. [CrossRef]
32. Vinken, G.C.M.; Boersma, K.F.; Maasakkers, J.D.; Adon, M.; Martin, R.V. Worldwide biogenic soil NOx emissions inferred from OMI NO_2 observations. *Atmos. Chem. Phys.* **2014**, *14*, 10363–10381. [CrossRef]
33. Lamsal, L.N.; Krotkov, N.A.; Vasilkov, A.; Marchenko, S.; Qin, W.; Yang, E.-S.; Fasnacht, Z.; Joiner, J.; Choi, S.; Haffner, D. OMI/aura nitrogen dioxide standard product with improved surface and cloud treatments. *Atmos. Meas. Tech. Discuss.* **2020**, *2020*, 1–56. [CrossRef]
34. Goldberg, D.L.; Anenberg, S.C.; Kerr, G.H.; Mohegh, A.; Lu, Z.; Streets, D.G. TROPOMI NO_2 in the United States: A Detailed Look at the Annual Averages, Weekly Cycles, Effects of Temperature, and Correlation With Surface NO_2 Concentrations. *Earths Future* **2021**, *9*, e2020EF001665. [CrossRef] [PubMed]
35. Veefkind, J.P.; Aben, I.; McMullan, K.; Förster, H.; De Vries, J.; Otter, G.; Claas, J.; Eskes, H.J.; De Haan, J.F.; Kleipool, Q.; et al. TROPOMI on the ESA Sentinel-5 Precursor: A GMES mission for global observations of the atmospheric composition for climate, air quality and ozone layer applications. *Remote Sens. Environ.* **2012**, *120*, 70–83. [CrossRef]
36. Inness, A.; Ades, M.; Agustí-Panareda, A.; Barré, J.; Benedictow, A.; Blechschmidt, A.-M.; Dominguez, J.J.; Engelen, R.; Eskes, H.; Flemming, J.; et al. The CAMS reanalysis of atmospheric composition. *Atmos. Chem. Phys.* **2019**, *19*, 3515–3556. [CrossRef]
37. Clerbaux, C.; Boynard, A.; Clarisse, L.; George, M.; Hadji-Lazaro, J.; Herbin, H.; Hurtmans, D.; Pommier, M.; Razavi, A.; Turquety, S.; et al. Monitoring of atmospheric composition using the thermal infrared IASI/MetOp sounder. *Atmos. Chem. Phys.* **2009**, *9*, 6041–6054.
38. Peuch, V.-H.; Engelen, R.; Rixen, M.; Dee, D.; Flemming, J.; Suttie, M.; Ades, M.; Agustí-Panareda, A.; Ananasso, C.; Andersson, E.; et al. The copernicus atmosphere monitoring service: From research to operations. *Bull. Am. Meteorol. Soc.* **2022**, *103*, E2650–E2668. [CrossRef]
39. Flemming, J.; Benedetti, A.; Inness, A.; Engelen, R.J.; Jones, L.; Huijnen, V.; Remy, S.; Parrington, M.; Suttie, M.; Bozzo, A.; et al. The CAMS interim reanalysis of carbon monoxide, ozone and aerosol for 2003–2015. *Atmos. Chem. Phys.* **2017**, *17*, 1945–1983. [CrossRef]
40. Kleipool, Q.; Rozemeijer, N.; van Hoek, M.; Leloux, J.; Loots, E.; Ludewig, A.; van der Plas, E.; Adrichem, D.; Harel, R.; Spronk, S.; et al. Ozone Monitoring Instrument (OMI) collection 4: Establishing a 17-year-long series of detrended level-1b data. *Atmos. Meas. Tech.* **2022**, *15*, 3527–3553.

Disclaimer/Publisher's Note: The statements, opinions and data contained in all publications are solely those of the individual author(s) and contributor(s) and not of MDPI and/or the editor(s). MDPI and/or the editor(s) disclaim responsibility for any injury to people or property resulting from any ideas, methods, instructions or products referred to in the content.